


## Fate of the superconducting state in floating islands of hybrid nanowire devices

E. V. Shpagina,<sup>1,2</sup> E. S. Tikhonov,<sup>1,2</sup> D. Ruhstorfer,<sup>3</sup> G. Koblmüller<sup>3</sup>,<sup>3</sup> and V. S. Khrapai<sup>1,2</sup>

<sup>1</sup>*Osipyan Institute of Solid State Physics, Russian Academy of Sciences, 142432 Chernogolovka, Russian Federation*

<sup>2</sup>*National Research University Higher School of Economics, 20 Myasnitskaya Street, 101000 Moscow, Russian Federation*

<sup>3</sup>*Walter Schottky Institut, Physik Department, and Center for Nanotechnology and Nanomaterials, Technische Universität München, Am Coulombwall 4, Garching 85748, Germany*

 (Received 20 November 2023; revised 6 February 2024; accepted 18 March 2024; published 1 April 2024)

We investigate the impact of transport current on the superconducting order parameter in superconducting islands in full-shell epitaxial Al-InAs nanowires. Depending on the device layout, the suppression of superconductivity occurs in three fundamentally different ways—by a critical current in the case of superconducting reservoirs and by a critical voltage or by a critical Joule power in the case of normal reservoirs. In the latter case, the collapse of the superconducting state depends on the ratio of the dwell time and the electron-phonon relaxation time of quasiparticles in the island. For low resistive and high resistive coupling to the reservoirs, respectively, a relaxation-free regime and a strong electron-phonon relaxation regime are realized. Our results shed light on the potential shortcomings of finite-bias transport spectroscopy in floating islands.

DOI: [10.1103/PhysRevB.109.L140501](https://doi.org/10.1103/PhysRevB.109.L140501)

Hybrid semiconductor-superconductor (semi-super) nanowires (NWs) are a lively research topic on the superconducting proximity effect, especially in its modern forefront—the Majorana research [1–3]. Such devices are investigated with the main focus on the semiconductor side and the quantities of interest include the induced spectral gap in the NW [4–9] and Andreev bound-state energies [8,10], the nonlocal response [11–20] and subgap heat conductance [15,17,18,21], the Josephson effect [22–29], a variety of zero-bias conductance anomalies [30–34], and Cooper-pair splitting [35–41]. Since typical currents in semi-super hybrids are orders of magnitude smaller than the critical current of the superconductor, the order parameter ( $\Delta$ ) is rarely a target for experimentalists beyond the equilibrium characterization [42]. As we show here, quasiparticle nonequilibrium and relaxation are much more relevant than current for the superconductivity in such devices.

In semi-super hybrids with a mesoscopic superconductor, which is not a part of the superconducting reservoir, referred to as the floating S-island below, the nonequilibrium mediated by the finite-bias voltage ( $V$ ) leads to a twofold complication. First, the quasiparticle population interplays with  $\Delta$ , since they are bound in the Bardeen-Cooper-Schrieffer (BCS) theory [43,44]. Second, this interplay may itself depend on the inelastic relaxation, provided quasiparticles spend enough time in the island [45–47]. Known in all-metal devices [48], nonequilibrium effects are not discussed in semi-super hybrids [49–55], with rare exceptions [56,57]. Clear indications of nonequilibrium effects were recently found in hybrid NWs at high biases  $|V| \gg \Delta/e$  [58,59]. The microscopic role of the energy relaxation in these experiments, however, remains hidden.

In this Letter we investigate the interplay of quasiparticle nonequilibrium, superconductivity, and electron-phonon (e-ph) relaxation in epitaxial full-shell Al-InAs NWs. Two device layouts are used, one with the S-island contacted di-

rectly (type-I devices) and the other with the S-island placed between the InAs segments (type-II devices). We demonstrate the suppression of superconductivity by critical current, critical voltage, or critical Joule power, as determined by the superconducting or normal state of the reservoirs and the quasiparticle dwell time in the island. Our experiments illuminate potential shortcomings of transport spectroscopy in floating S-islands related to nonequilibrium superconductivity.

Samples used in this study are fabricated from nominally identical InAs NWs grown by molecular beam epitaxy, with an *in situ* deposited Al shell fully surrounding the NW. A scanning electron micrograph of the as-grown NW array is given in Fig. 1(a) with further growth details provided in the Supplemental Material (SM) [60]. Individual NWs are dry-transferred with a home-made micromanipulator onto prepatterned  $\sim 150$ -nm-thick Au pads, which serve to align and suspend NWs above the Si/SiO<sub>2</sub> substrate. Transport and noise measurements are performed in a quasi-four-point setup in a <sup>3</sup>He cryostat at base temperatures of  $T_0 \approx 0.45$ – $0.5$  K with the sample immersed in liquid. Altogether we studied two type-I devices and five type-II devices with very similar results among each group.

We start from superconducting properties in equilibrium, characterized in type-I devices. Here, ohmic contacts are established directly to the shell [see the sample layout and contact cross section in Fig. 1(b)]. A high-quality interface between epitaxial aluminum (epi-Al) and 250-nm-thick e-gun evaporated aluminum (evap-Al) is achieved via *in situ* Ar milling. Figure 1(c) is a color-scale plot of the linear response resistance ( $R$ ) in device IA as a function of  $B$  and  $T$  (cooldown 2). Three regimes are identified: a normal high- $T$  regime, a superconducting low- $T$  and low- $B$  regime (SSS), and an intermediate regime with a superconducting shell and normal contacts (NSN). The regimes change at the transitions of the epi-Al and evap-Al from the normal to the superconducting

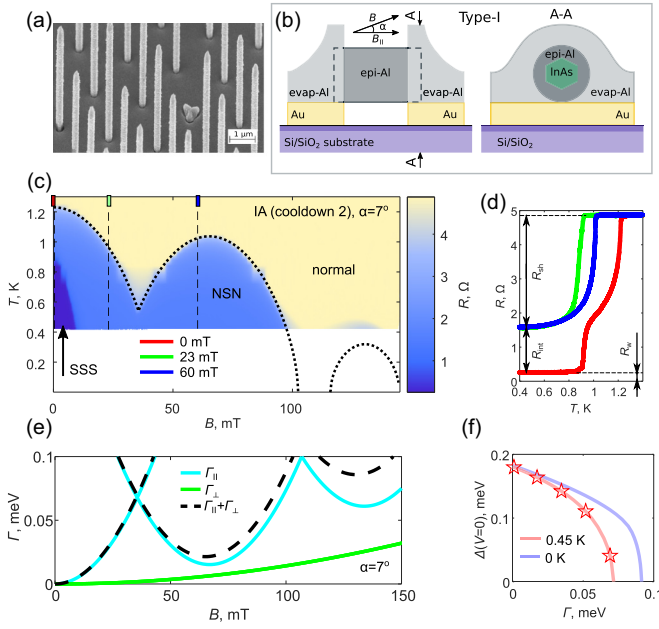


FIG. 1. Superconductivity in equilibrium in type-I devices. (a) Scanning electron micrograph of the as-grown Al-InAs NW array. (b) Schematic layout of a type-I device and cross section in the contact region. (c) Color-scale plot of  $R(B, T)$  in device IA (cooldown 2). The dotted line is the fit to  $T_c(B)$  of the epi-Al. (d)  $R(T)$  traces at fixed  $B$  fields, corresponding to the vertical dashed lines in (c). (e) Depairing factors  $\Gamma$ ,  $\Gamma_{\parallel}$ , and  $\Gamma_{\perp}$  as a function of the  $B$  field, calculated to fit the data in (c). (f) Superconducting order parameter in dependence of  $\Gamma$  at two different temperatures (see legend). Discrete points  $\Delta(\Gamma)$  marked by stars are the same as in Fig. 2(d).

state, with representative  $R(T)$  curves displayed in Fig. 1(d). In  $B = 0$  (red line)  $R(T)$  exhibits two steps at the critical temperatures ( $T_c$ ) of the epi-Al ( $T_c^0 \approx 1.23$  K) and evap-Al ( $T_c \approx 0.95$  K). In the latter case, the reduced  $T_c$  is a result of the inverse proximity effect from the Au layer. At lower  $T$  the resistance saturates at  $R_w \approx 0.26 \Omega$ , which we attribute to the wiring contribution. Two other traces taken above the critical  $B$  field of the evap-Al show only a single step on the  $R(T)$  at the  $T_c$  of the epi-Al. These data give the resistances of evap-Al/epi-Al interfaces  $R_{\text{int}} \approx 1.3 \Omega$  and of the epi-Al shell  $R_{\text{sh}} \approx 3.3 \Omega$ . As shown in the SM [60], a series contribution of the contact pads in  $R_{\text{int}}$  is negligible.

The  $T_c$  of the epi-Al in Fig. 1(c) exhibits Little-Parks (LP) oscillations in the  $B$  field, which enables to extract the microscopic parameters of the shell. The dependence of  $T_c(B)$  is controlled by the depairing factor  $\Gamma = \Gamma_{\parallel} + \Gamma_{\perp}$ , which has contributions from parallel ( $B_{\parallel} \approx B$ ) and perpendicular ( $B_{\perp} \approx \alpha B$ ) components of the  $B$  field. Here,  $\alpha$  is a small angle between the NW axis and the  $B$  field, which is not controlled in the experiment and treated as a fit parameter, separately in each device and in each cooldown. In our calculations we closely follow the Usadel theory in the formalism of Ref. [61] (see the SM [60] for the details). The  $T_c(B)$  is found from the Abrikosov-Gorkov equation [42,59] [dotted line in Fig. 1(c)].  $\Gamma$  is derived in the approximation of a cylindrical shell with an inner radius of  $\rho_i$  and thickness of  $t$ , without the assumption that  $t \ll \rho_i$ . The best fits provide  $\rho_i = 80 \pm 4$  nm,  $t = 42$

nm, and diffusion coefficient  $D = 69$  cm<sup>2</sup>/s. The order parameter  $\Delta_0 \approx 187 \mu\text{eV}$  and the superconducting coherence length  $\xi_0 \equiv \sqrt{\hbar D / \Delta_0} \approx 156$  nm in the limit of  $B = 0$ ,  $T = 0$  are obtained from the BCS relation  $\Delta_0 \approx 1.76 k_B T_c^0$ . The calculated dependencies  $\Gamma(B)$  in device IA (cooldown 2) in different LP lobes and  $\Delta(\Gamma)$  for  $T = T_0$  and  $T = 0$  are plotted, respectively, in Figs. 1(e) and 1(f).

Next, we investigate the fate of shell superconductivity in response to transport current ( $I$ ). Here, three different scenarios can be expected. In devices with superconducting reservoirs directly contacting the shell, the superconductivity breaks down in a conventional way at the shell critical current  $I_c$ . This is realized in type-I devices in the SSS regime. In devices with normal reservoirs, the resistance is always finite and quasiparticle nonequilibrium plays a crucial role [43]. The electronic energy distribution [EED,  $f(\varepsilon)$ ] is then determined by a competition between finite  $V$  and energy relaxation. Without relaxation,  $f(\varepsilon)$  is a nonequilibrium double-step  $f_{\text{NEQ}}(V) = [f_0(\varepsilon - V/2, T_0) + f_0(\varepsilon + V/2, T_0)]/2$ , where  $f_0(\varepsilon, T)$  is the Fermi-Dirac EED at a given  $T$ . This EED implies symmetric coupling to the reservoirs [43,44], that agrees with the experimental data. For strong relaxation, local equilibrium is achieved with  $f_{\text{LEQ}}(T_e) = f_0(\varepsilon, T_e)$ , where  $T_e > T_0$  is the electronic temperature in the island. In the first case the superconductivity is destroyed at a critical voltage [43,44,48,57]  $|V_C| \sim \Delta/e$ , whereas in the second case it collapses at  $T_e = T_c$ . The two limiting cases are realized, respectively, in type-I and type-II devices. Figure 2 summarizes the nonequilibrium response in type-I device IA (cooldown 1). Figure 2(a) is a color-scale plot of the differential resistance  $R_{\text{diff}} = dV^*/dI$  at  $T = T_0$  in dependence on  $B$  and  $I$ , with the current sweep direction indicated by the arrow. Here,  $V^* \equiv V - IR_w$  is the actual bias on the device with a subtracted wiring contribution. Vertical dashed lines correspond to  $I-V^*$  curves displayed in Fig. 2(b) for both sweep directions. A superconducting behavior with  $V^* \approx 0$  is found in the SSS regime (upper panel), whereas finite-resistance superconductivity is evident in the NSN regime (lower panel). In both cases, the usual huge hysteresis is found [48]. We are interested in a suppression of the superconducting state, which occurs at increasing  $|V^*|$  and is manifested by a single jump on the  $I-V^*$  curves. Critical voltages  $V_C^*$  measured right before this jump are exemplified by circles in Fig. 2(b). Symbols in Fig. 2(c) display the  $B$ -field evolution of  $V_C^*$  in device IA (two cooldowns) and in device IB. In the SSS regime, a small residual voltage is measured, possibly originating from phase slips or vortices in  $B_{\perp} \neq 0$ , thus the superconductivity is destroyed in a conventional way at a critical current. The value of  $I_c(B = 0) \approx 0.35$  mA is a factor of 2 smaller compared to the thermodynamical critical current of the epi-Al, the difference most likely coming from the interface resistance (see the SM [60]). By contrast, in the NSN regime the superconductivity collapses at smaller  $I$  and at  $V_C^* \sim \Delta/e$ . The measured  $V_C^*(B)$  is consistent among the devices and cooldowns, with deviations at higher  $B$  fields caused by variations of  $\alpha$ .

We explain the evolution of  $V_C^*(B)$  in the NSN regime by the Usadel theory, taking into account the nonequilibrium EED in the spirit of Ref. [43]. We find the solution in the depth of the S-island, at distances larger than  $\xi_0$  from the ends,

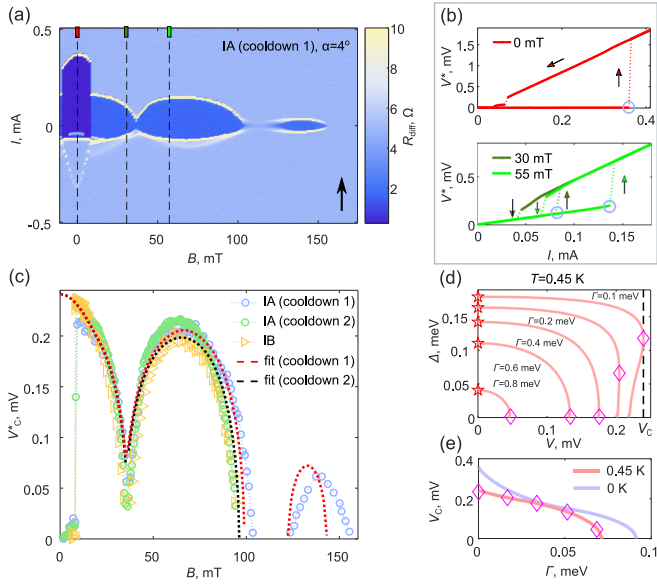


FIG. 2. Nonequilibrium in type-I devices. (a) Color-scale plot of  $R_{\text{diff}}(B, I)$  in device IA (cooldown 1) for the current sweep direction indicated by an arrow. (b)  $I$ - $V^*$  curves taken at fixed  $B$ -field values in the SSS and NSN regimes for both current sweep directions (arrows). The  $B$  fields are indicated in the legends and correspond to the vertical dashed lines in (a). (c) Critical voltage extracted from the  $I$ - $V^*$  curves for device IA in two cooldowns and device IB (symbols). Dashed lines are fits to the data in device IA. (d) Calculated dependencies  $\Delta(V)$  for a set of  $\Gamma$ , used to obtain the equilibrium order parameter (stars) and critical voltage (diamonds). The dashed line represents  $V_C$  for  $\Gamma = 0.1$  meV. (e) Calculated  $V_C(\Gamma)$  at  $T = T_0$  and  $T = 0$ , reproducing the data from (d) (diamonds).

where the charge imbalance decays and the nonequilibrium EED is of the form  $f_{\text{NEQ}}(V)$ . A self-consistent numerical procedure to find  $\Delta(V)$  is detailed in the SM [60]. Figure 2(d) shows the results for a set of  $\Gamma$  (solid lines). The data in equilibrium ( $V = 0$ ) are the same as in Fig. 1(f) (stars). At increasing  $V$ ,  $\Delta$  gets suppressed, so that no solution exists above certain  $V_C$  (diamonds, dashed line). At small  $\Gamma$  the solution is bistable just below  $V_C$ , consistent with previous results [43,44,48,57]. Calculated  $V_C(\Gamma)$  is shown in Fig. 2(e) along with the symbols from Fig. 2(d). Using the  $\Gamma$ - $B$  correspondence the dependencies  $V_C(B)$  are obtained and plotted in Fig. 2(c) for device IA in two cooldowns (dashed lines). Near perfect agreement with the experiment ensures that the relaxation-free scenario of nonequilibrium superconductivity is realized in type-I devices.

We now switch to type-II devices, where the selectively etched shell forms a floating S-island of length  $L = 0.5$ – $2$   $\mu\text{m}$  [see the micrograph and sketch in Figs. 3(a) and 3(b)]. Ohmic contacts are defined via evaporation of Cr/Au with *ex situ* passivation of the native oxide in ammonium polysulfide [6,25,62]. Owing to the InAs segments, the device resistance is about four orders of magnitude higher than  $R_{\text{int}}$  in type-I devices and is controllable by the back-gate voltage  $V_g$ . Figures 3(c) and 3(d), respectively, the color-scale plot  $R_{\text{diff}}(I, B)$  in device IIA and representative traces  $R_{\text{diff}}(V)$  at fixed  $B$ , corresponding to vertical dashed lines in the color plot. The low-bias behavior of  $R_{\text{diff}}$  is a combination of the

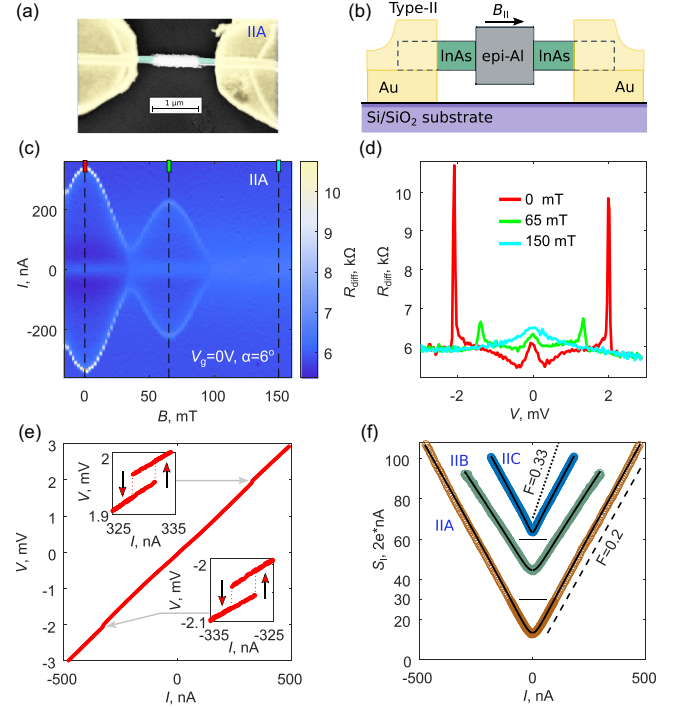


FIG. 3. Nonequilibrium in type-II devices. (a), (b) Electron micrograph of device IIA (false colors) and schematic layout of type-II devices. (c) Color-scale plot of  $R_{\text{diff}}(B, I)$  in device IIA. (d) Bias dependencies of  $R_{\text{diff}}$  at fixed  $B$  fields, corresponding to the dashed lines in (c). (e)  $I$ - $V$  curve measured at  $B = 0$ , showing tiny voltage jumps at high biases  $V \approx 2$  mV. Insets magnify these features, demonstrating weak hysteresis with respect to the current sweep direction. (f) Noise spectral density in devices IIA, IIB, and IIC as a function of  $I$  in the normal transport regime at high enough  $B$  (symbols). Two upper traces are shifted upward for clarity, with zero levels marked by thin solid lines. Dashed and dotted guide lines have slopes corresponding to Fano factors of  $F = 0.2$  and  $F_D = 1/3$ , respectively. Solid lines are fits taking into account the relaxation in the S-island (see the SM [60]).

superconducting proximity effect in diffusive NS junctions with a nonideal interface [7,15,18], observable at low  $B$  fields, and Coulomb effects [63–65], which contribute a broad zero-bias resistance maximum, observable at high  $B$  fields. We do not discuss these device-specific and  $V_g$ -dependent properties and concentrate on a sharp resistance peak observed in all devices at much higher  $V$ . The LP oscillations of the peak position [Fig. 3(c)], and the tiny voltage jump from which the peak originates [Fig. 3(e)] show that this feature is associated with the collapse of superconductivity. Corresponding voltage jumps are most pronounced at  $B = 0$  and demonstrate weak hysteresis [see the insets of Fig. 3(e)]. At increasing  $B$  they smear out and the visibility of the LP oscillations reduces [Fig. 3(c)].

The observation of a superconducting state at voltages  $|V| \gg \Delta/e$  implies strong energy relaxation. Otherwise, as found in type-I devices, the double-step EED  $f_{\text{NEQ}}(V)$  in the S-island would not be compatible with the superconductivity. Although in the type-II devices a moderate asymmetry of the couplings to the reservoirs can affect the EED and reduce the effect of nonequilibrium [44,57], it is too weak to maintain

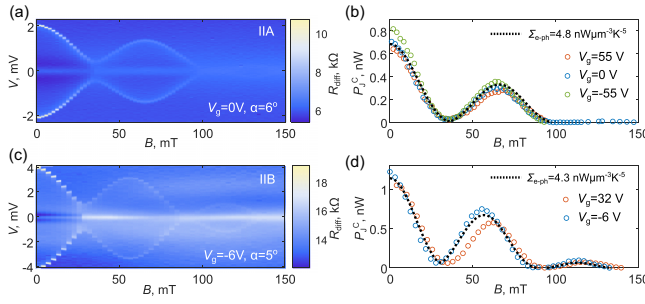


FIG. 4. Critical Joule power in type-II devices. (a) Color-scale plot of  $R_{\text{diff}}(B, V)$  in device IIA ( $V_g$  and  $\alpha$  indicated in the legend). (b)  $B$  dependencies of the critical Joule power for the same device (symbols) and the fit to the e-ph relaxation model (dashed line). Gate voltages and the e-ph cooling power are indicated in the legend. (c), (d) The same in device IIB.

the superconducting state at mV-range biases. A direct test of the relaxation is achieved via shot-noise measurements in the normal state, shown in Fig. 3(f) (see SM [60] for the details). The noise spectral density (symbols) exhibits a shot-noise behavior  $S_1 \approx 2eFI$  with Fano factors  $F \approx 0.2$  (dashed line). This value is considerably reduced compared to the universal  $F_D = 1/3$  in diffusive conductors without relaxation [66,67], usually found in InAs NWs [18,68,69] (dotted line). The reduction of  $F$  is a result of strong e-ph relaxation in the S-island [70]. We assume local equilibrium EED  $f_{\text{LEQ}}(T_e)$  with the electronic temperature, which obeys the heat balance equation  $\frac{1}{2}P_j = \mathcal{V}_{\text{Al}} \Sigma_{\text{e-ph}}(T_e^5 - T_0^5)$ . Here,  $P_j \equiv IV$  is the Joule power released in the semiconducting segments, half of which is dissipated in the S-island,  $\mathcal{V}_{\text{Al}}$  is the volume of the epi-Al, and  $\Sigma_{\text{e-ph}}$  is the e-ph cooling power. Note a conceptual difference from Ref. [59], in which the Joule power flows into the reservoirs by the electronic heat conduction, while the e-ph relaxation is neglected. The above equation simultaneously explains the shot noise in Fig. 3(f) (solid lines) and the suppression of superconductivity by transport current. In the latter case, the superconductivity collapses at the critical Joule power ( $P_j^c$ ), which corresponds to  $T_e = T_c(B)$ . The dependencies  $P_j^c(B)$  in devices IIA and IIB are shown in Figs. 4(b) and 4(d) (symbols) and correspond, respectively, to the color plots in Figs. 4(a) and 4(c). We fit the data in these and other devices with similar  $\Sigma_{\text{e-ph}} \approx 4.8 \pm 1 \text{ nW } \mu\text{m}^{-3} \text{ K}^{-5}$ ; see the dashed lines (more data in the SM [60]). This value corresponds to the

e-ph relaxation time of  $\tau_{\text{e-ph}} \approx 60 \text{ ns}$  at  $T = T_0$ , in agreement with independent measurements in aluminum [71].

The origin of different behavior in type-I and type-II devices is in the ratio of quasiparticle dwell time in the S-island  $\tau_{\text{dwell}}$ , controlled by the coupling to the reservoirs, and  $\tau_{\text{e-ph}}$ . Type-I devices are strongly coupled to reservoirs and the dwell time is mainly limited by diffusion  $\tau_{\text{dwell}}^{\text{I}} \sim L^2/D \approx 1 \text{ ns}$  for the typical  $L \approx 3 \mu\text{m}$ . In type-II devices  $L$  is smaller, however, the coupling to reservoirs is very weak owing to highly resistive InAs segments. Thus, the dwell time is renormalized by the ratio of the numbers of the eigenmodes in epi-Al and in InAs or, roughly, by the ratio of semiconductor and superconductor resistances in the normal state ( $\sim 10^4$ ), giving  $\tau_{\text{dwell}}^{\text{II}} \sim 1 \mu\text{s}$ . The relation  $\tau_{\text{dwell}}^{\text{I}} \ll \tau_{\text{e-ph}} \ll \tau_{\text{dwell}}^{\text{II}}$  naturally explains the relaxation-free regime in type-I devices and strong relaxation regime in type-II devices. Semi-super research usually deals with superconducting islands analogous to our type-II devices [49–52,54,55,72]. It is illuminating to discuss how such systems could fall in the nonequilibrium regime observed in type-I devices. A sizable decrease of the  $\tau_{\text{dwell}}$  by populating more conduction channels is not feasible in semiconducting NWs. Figures 4(b) and 4(d) demonstrate a weak  $V_g$  dependence of  $P_j^c$ , indicating only minor deviations from local equilibrium in our experiment. Note, however, that lowering the temperature leads to the increase of  $\tau_{\text{e-ph}} \propto T^{-3}$  so that energy relaxation slows down significantly. Critical voltages on the order of  $\Delta/e$  found at mK temperatures in a recent study [73] may indicate the relevance of nonequilibrium.

In summary, our results illuminate the way in which the superconducting order parameter and the bias and relaxation controlled quasiparticle population are bound with each other in floating S-islands. This binding indicates a general shortcoming of the transport spectroscopy in semi-super hybrids, since the quasiparticle excitation spectrum becomes dependent on the bias voltage and relaxation.

We acknowledge the valuable advice of Ya. V. Fominov and A. S. Mel'nikov on the Usadel theory and the fabrication help of S. V. Egorov. We thank A. V. Bubis for his input on the early stages of this work and for useful remarks. V.S.K. is grateful to T. M. Klapwijk for early illuminating discussions of nonequilibrium superconductivity. This work was supported by the Russian Science Foundation Project No. 22-12-00342.

- [1] R. M. Lutchyn, J. D. Sau, and S. Das Sarma, Majorana fermions and a topological phase transition in semiconductor-superconductor heterostructures, *Phys. Rev. Lett.* **105**, 077001 (2010).
- [2] Y. Oreg, G. Refael, and F. von Oppen, Helical liquids and Majorana bound states in quantum wires, *Phys. Rev. Lett.* **105**, 177002 (2010).
- [3] E. Prada, P. San-Jose, M. W. A. de Moor, A. Geresdi, E. J. H. Lee, J. Klinovaja, D. Loss, J. Nygård, R. Aguado, and L. P. Kouwenhoven, From Andreev to Majorana bound states in hybrid superconductor–semiconductor nanowires, *Nat. Rev. Phys.* **2**, 575 (2020).
- [4] W. Chang, S. M. Albrecht, T. S. Jespersen, F. Kuemmeth, P. Krogstrup, J. Nygård, and C. M. Marcus, Hard gap in epitaxial semiconductor–superconductor nanowires, *Nat. Nanotechnol.* **10**, 232 (2015).
- [5] P. Krogstrup, N. L. B. Ziino, W. Chang, S. M. Albrecht, M. H. Madsen, E. Johnson, J. Nygård, C. M. Marcus, and T. S. Jespersen, Epitaxy of semiconductor–superconductor nanowires, *Nat. Mater.* **14**, 400 (2015).
- [6] Ö. Gül, H. Zhang, F. K. de Vries, J. van Veen, K. Zuo, V. Mourik, S. Conesa-Boj, M. P. Nowak, D. J. van Woerkom, M. Quintero-Pérez, M. C. Cassidy, A. Geresdi, S. Koelling, D. Car, S. R. Plissard, E. P. A. M. Bakkers, and L. P. Kouwenhoven,

- Hard superconducting gap in InSb nanowires, *Nano Lett.* **17**, 2690 (2017).
- [7] A. V. Bubis, Proximity effect and interface transparency in Al/InAs-nanowire/Al diffusive junctions, *Semicond. Sci. Technol.* **32**, 094007 (2017).
- [8] C. Jünger, R. Delagrangé, D. Chevallier, S. Lehmann, K. A. Dick, C. Thelander, J. Klinovaja, D. Loss, A. Baumgartner, and C. Schönenberger, Magnetic-field-independent subgap states in hybrid Rashba nanowires, *Phys. Rev. Lett.* **125**, 017701 (2020).
- [9] P. Yu, B. D. Woods, J. Chen, G. Badawy, E. P. A. M. Bakkers, T. D. Stanescu, and S. M. Frolov, Delocalized states in three-terminal superconductor-semiconductor nanowire devices, *SciPost Phys.* **15**, 005 (2023).
- [10] C. Jünger, A. Baumgartner, R. Delagrangé, D. Chevallier, S. Lehmann, M. Nilsson, K. A. Dick, C. Thelander, and C. Schönenberger, Spectroscopy of the superconducting proximity effect in nanowires using integrated quantum dots, *Commun. Phys.* **2**, 76 (2019).
- [11] T. D. Stanescu and S. Tewari, Nonlocality of zero-bias anomalies in the topologically trivial phase of Majorana wires, *Phys. Rev. B* **89**, 220507(R) (2014).
- [12] T. Ö. Rosdahl, A. Vuik, M. Kjaergaard, and A. R. Akhmerov, Andreev rectifier: A nonlocal conductance signature of topological phase transitions, *Phys. Rev. B* **97**, 045421 (2018).
- [13] Y.-H. Lai, J. D. Sau, and S. Das Sarma, Presence versus absence of end-to-end nonlocal conductance correlations in Majorana nanowires: Majorana bound states versus Andreev bound states, *Phys. Rev. B* **100**, 045302 (2019).
- [14] G. C. Ménard, G. L. R. Anselmetti, E. A. Martinez, D. Puglia, F. K. Malinowski, J. S. Lee, S. Choi, M. Pendharkar, C. J. Palmstrøm, K. Flensberg, C. M. Marcus, L. Casparis, and A. P. Higginbotham, Conductance-matrix symmetries of a three-terminal hybrid device, *Phys. Rev. Lett.* **124**, 036802 (2020).
- [15] A. O. Denisov, A. V. Bubis, S. U. Piatrusha, N. A. Titova, A. G. Nasibulin, J. Becker, J. Treu, D. Ruhstorfer, G. Koblmüller, E. S. Tikhonov, and V. S. Khrapai, Charge-neutral nonlocal response in superconductor-InAs nanowire hybrid devices, *Semicond. Sci. Technol.* **36**, 09LT04 (2021).
- [16] D. Puglia, E. A. Martinez, G. C. Ménard, A. Pöschl, S. Gronin, G. C. Gardner, R. Kallaher, M. J. Manfra, C. M. Marcus, A. P. Higginbotham, and L. Casparis, Closing of the induced gap in a hybrid superconductor-semiconductor nanowire, *Phys. Rev. B* **103**, 235201 (2021).
- [17] H. Pan, J. D. Sau, and S. Das Sarma, Three-terminal nonlocal conductance in Majorana nanowires: Distinguishing topological and trivial in realistic systems with disorder and inhomogeneous potential, *Phys. Rev. B* **103**, 014513 (2021).
- [18] A. Denisov, A. Bubis, S. Piatrusha, N. Titova, A. Nasibulin, J. Becker, J. Treu, D. Ruhstorfer, G. Koblmüller, E. Tikhonov, and V. Khrapai, Heat-mode excitation in a proximity superconductor, *Nanomaterials* **12**, 1461 (2022).
- [19] G. Wang, T. Dvir, N. van Loo, G. P. Mazur, S. Gazibegovic, G. Badawy, E. P. A. M. Bakkers, L. P. Kouwenhoven, and G. de Lange, Nonlocal measurement of quasiparticle charge and energy relaxation in proximitized semiconductor nanowires using quantum dots, *Phys. Rev. B* **106**, 064503 (2022).
- [20] A. Kejriwal and B. Muralidharan, Nonlocal conductance and the detection of Majorana zero modes: Insights from von Neumann entropy, *Phys. Rev. B* **105**, L161403 (2022).
- [21] A. R. Akhmerov, J. P. Dahlhaus, F. Hassler, M. Wimmer, and C. W. J. Beenakker, Quantized conductance at the Majorana phase transition in a disordered superconducting wire, *Phys. Rev. Lett.* **106**, 057001 (2011).
- [22] T. Nishio, T. Kozakai, S. Amaha, M. Larsson, H. A. Nilsson, H. Q. Xu, G. Zhang, K. Tateno, H. Takayanagi, and K. Ishibashi, Supercurrent through InAs nanowires with highly transparent superconducting contacts, *Nanotechnology* **22**, 445701 (2011).
- [23] S. Abay, H. Nilsson, F. Wu, H. Xu, C. Wilson, and P. Delsing, High critical-current superconductor-InAs nanowire-superconductor junctions, *Nano Lett.* **12**, 5622 (2012).
- [24] S. Abay, D. Persson, H. Nilsson, F. Wu, H. Q. Xu, M. Fogelström, V. Shumeiko, and P. Delsing, Charge transport in InAs nanowire Josephson junctions, *Phys. Rev. B* **89**, 214508 (2014).
- [25] J. Paajaste, M. Amado, S. Roddaro, F. S. Bergeret, D. Ercolani, L. Sorba, and F. Giazotto, Pb/InAs nanowire Josephson junction with high critical current and magnetic flux focusing, *Nano Lett.* **15**, 1803 (2015).
- [26] P. Perla, Fully in situ Nb/InAs-nanowire Josephson junctions by selective-area growth and shadow evaporation, *Nanoscale Adv.* **3**, 1413 (2021).
- [27] B. Kousar, D. J. Carrad, L. Stampfer, P. Krogstrup, J. Nygård, and T. S. Jespersen, InAs/MoRe hybrid semiconductor/superconductor nanowire devices, *Nano Lett.* **22**, 8845 (2022).
- [28] E. M. Spanton, M. Deng, S. Vaitiekėnas, P. Krogstrup, J. Nygård, C. M. Marcus, and K. A. Moler, Current-phase relations of few-mode InAs nanowire Josephson junctions, *Nat. Phys.* **13**, 1177 (2017).
- [29] S. Hart, Current-phase relations of InAs nanowire Josephson junctions: From interacting to multimode regimes, *Phys. Rev. B* **100**, 064523 (2019).
- [30] A. Das, Y. Ronen, Y. Most, Y. Oreg, M. Heiblum, and H. Shtrikman, Zero-bias peaks and splitting in an Al-InAs nanowire topological superconductor as a signature of Majorana fermions, *Nat. Phys.* **8**, 887 (2012).
- [31] V. Mourik, K. Zuo, S. M. Frolov, S. R. Plissard, E. P. A. M. Bakkers, and L. P. Kouwenhoven, Signatures of Majorana fermions in hybrid superconductor-semiconductor nanowire devices, *Science* **336**, 1003 (2012).
- [32] S. Vaitiekėnas, G. W. Winkler, B. Van Heck, T. Karzig, M.-T. Deng, K. Flensberg, L. I. Glazman, C. Nayak, P. Krogstrup, R. M. Lutchyn, and C. M. Marcus, Flux-induced topological superconductivity in full-shell nanowires, *Science* **367**, eaav3392 (2020).
- [33] S. Vaitiekėnas, Y. Liu, P. Krogstrup, and C. M. Marcus, Zero-bias peaks at zero magnetic field in ferromagnetic hybrid nanowires, *Nat. Phys.* **17**, 43 (2021).
- [34] M. Valentini, F. Peñaranda, A. Hofmann, M. Brauns, R. Hauschild, P. Krogstrup, P. San-Jose, E. Prada, R. Aguado, and G. Katsaros, Nontopological zero-bias peaks in full-shell nanowires induced by flux-tunable Andreev states, *Science* **373**, 82 (2021).
- [35] L. Hofstetter, S. Csonka, J. Nygård, and C. Schönenberger, Cooper pair splitter realized in a two-quantum-dot Y-junction, *Nature (London)* **461**, 960 (2009).

- [36] L. G. Herrmann, F. Portier, P. Roche, A. L. Yeyati, T. Kontos, and C. Strunk, Carbon nanotubes as Cooper-pair beam splitters, *Phys. Rev. Lett.* **104**, 026801 (2010).
- [37] A. Das, Y. Ronen, M. Heiblum, D. Mahalu, A. V. Kretinin, and H. Shtrikman, High-efficiency Cooper pair splitting demonstrated by two-particle conductance resonance and positive noise cross-correlation, *Nat. Commun.* **3**, 1165 (2012).
- [38] S. Baba, C. Jünger, S. Matsuo, A. Baumgartner, Y. Sato, H. Kamata, K. Li, S. Jeppesen, L. Samuelson, H. Xu, C. Schönberger, and S. Tarucha, Cooper-pair splitting in two parallel InAs nanowires, *New J. Phys.* **20**, 063021 (2018).
- [39] G. Wang, T. Dvir, G. P. Mazur, C.-X. Liu, N. Van Loo, S. L. D. Ten Haaf, A. Bordin, S. Gazibegovic, G. Badawy, E. P. A. M. Bakkers, M. Wimmer, and L. P. Kouwenhoven, Singlet and triplet Cooper pair splitting in hybrid superconducting nanowires, *Nature (London)* **612**, 448 (2022).
- [40] A. Bordoloi, V. Zannier, L. Sorba, C. Schönberger, and A. Baumgartner, Spin cross-correlation experiments in an electron entangler, *Nature (London)* **612**, 454 (2022).
- [41] Z. Scherübl, G. Fülöp, J. Gramich, A. Pályi, C. Schönberger, J. Nygård, and S. Csonka, From Cooper pair splitting to the non-local spectroscopy of a Shiba state, *Phys. Rev. Res.* **4**, 023143 (2022).
- [42] S. Vaitiekėnas, P. Krogstrup, and C. M. Marcus, Anomalous metallic phase in tunable destructive superconductors, *Phys. Rev. B* **101**, 060507(R) (2020).
- [43] R. S. Keizer, M. G. Flokstra, J. Aarts, and T. M. Klapwijk, Critical voltage of a mesoscopic superconductor, *Phys. Rev. Lett.* **96**, 147002 (2006).
- [44] I. Snyman and Yu. V. Nazarov, Bistability in voltage-biased normal-metal/insulator/superconductor/insulator/normal-metal structures, *Phys. Rev. B* **79**, 014510 (2009).
- [45] B. Huard, H. Pothier, D. Esteve, and K. E. Nagaev, Electron heating in metallic resistors at sub-Kelvin temperature, *Phys. Rev. B* **76**, 165426 (2007).
- [46] E. Sivre, A. Anthore, F. D. Parmentier, A. Cavanna, U. Gennser, A. Ouerghi, Y. Jin, and F. Pierre, Heat Coulomb blockade of one ballistic channel, *Nat. Phys.* **14**, 145 (2018).
- [47] A. Rosenblatt, S. Konyzheva, F. Lafont, N. Schiller, J. Park, K. Snizhko, M. Heiblum, Y. Oreg, and V. Umansky, Energy relaxation in edge modes in the quantum Hall effect, *Phys. Rev. Lett.* **125**, 256803 (2020).
- [48] N. Vercruyssen, T. G. A. Verhagen, M. G. Flokstra, J. P. Pekola, and T. M. Klapwijk, Evanescent states and nonequilibrium in driven superconducting nanowires, *Phys. Rev. B* **85**, 224503 (2012).
- [49] L. Fu, Electron teleportation via Majorana bound states in a mesoscopic superconductor, *Phys. Rev. Lett.* **104**, 056402 (2010).
- [50] J. Ulrich and F. Hassler, Majorana-assisted nonlocal electron transport through a floating topological superconductor, *Phys. Rev. B* **92**, 075443 (2015).
- [51] S. M. Albrecht, A. P. Higginbotham, M. Madsen, F. Kuemmeth, T. S. Jespersen, J. Nygård, P. Krogstrup, and C. M. Marcus, Exponential protection of zero modes in Majorana islands, *Nature (London)* **531**, 206 (2016).
- [52] Y.-H. Lai, S. Das Sarma, and J. D. Sau, Theory of Coulomb blocked transport in realistic Majorana nanowires, *Phys. Rev. B* **104**, 085403 (2021).
- [53] Y. Hao, G. Zhang, D. Liu, and D. E. Liu, Double F teleportation and anomalous Coulomb blockade in a Majorana-hosted superconducting island, *Nat. Commun.* **13**, 6699 (2022).
- [54] R. S. Souto, M. M. Wauters, K. Flensberg, M. Leijnse, and M. Burrello, Multiterminal transport spectroscopy of subgap states in Coulomb-blockaded superconductors, *Phys. Rev. B* **106**, 235425 (2022).
- [55] M. Valentini, M. Borovkov, E. Prada, S. Martí-Sánchez, M. Botifoll, A. Hofmann, J. Arbiol, R. Aguado, P. San-Jose, and G. Katsaros, Majorana-like Coulomb spectroscopy in the absence of zero-bias peaks, *Nature (London)* **612**, 442 (2022).
- [56] S. Roddaro, A. Pescaglioni, D. Ercolani, L. Sorba, F. Giazotto, and F. Beltram, Hot-electron effects in InAs nanowire Josephson junctions, *Nano Res.* **4**, 259 (2011).
- [57] A. V. Bubis, E. V. Shpagina, A. G. Nasibulin, and V. S. Khrapai, Thermal conductance and nonequilibrium superconductivity in a diffusive NSN wire probed by shot noise, *Phys. Rev. B* **104**, 125409 (2021).
- [58] M.-L. Liu, D. Pan, T. Le, J.-B. He, Z.-M. Jia, S. Zhu, G. Yang, Z.-Z. Lyu, G.-T. Liu, J. Shen, J.-H. Zhao, L. Lu, and F.-M. Qu, Gate-tunable negative differential conductance in hybrid semiconductor–superconductor devices, *Chin. Phys. Lett.* **40**, 067301 (2023).
- [59] A. Ibabe, M. Gómez, G. O. Steffensen, T. Kanne, J. Nygård, A. L. Yeyati, and E. J. H. Lee, Joule spectroscopy of hybrid superconductor–semiconductor nanodevices, *Nat. Commun.* **14**, 2873 (2023).
- [60] See Supplemental Materials at <http://link.aps.org/supplemental/10.1103/PhysRevB.109.L140501> for the details of growth, experiment and theoretical calculations, which also includes Refs. [74–77].
- [61] A. Anthore, H. Pothier, and D. Esteve, Density of states in a superconductor carrying a supercurrent, *Phys. Rev. Lett.* **90**, 127001 (2003).
- [62] M. J. L. Sourribes, I. Isakov, M. Panfilova, and P. A. Warburton, Minimization of the contact resistance between InAs nanowires and metallic contacts, *Nanotechnology* **24**, 045703 (2013).
- [63] Y. V. Nazarov, Coulomb blockade without tunnel junctions, *Phys. Rev. Lett.* **82**, 1245 (1999).
- [64] D. S. Golubev and A. D. Zaikin, Coulomb interaction and quantum transport through a coherent scatterer, *Phys. Rev. Lett.* **86**, 4887 (2001).
- [65] A. Levy Yeyati, A. Martin-Rodero, D. Esteve, and C. Urbina, Direct link between Coulomb blockade and shot noise in a quantum-coherent structure, *Phys. Rev. Lett.* **87**, 046802 (2001).
- [66] K. Nagaev, On the shot noise in dirty metal contacts, *Phys. Lett. A* **169**, 103 (1992).
- [67] C. W. J. Beenakker and M. Buttiker, Suppression of shot noise in metallic diffusive conductors, *Phys. Rev. B* **46**, 1889 (1992).
- [68] E. S. Tikhonov, D. V. Shovkun, D. Ercolani, F. Rossella, M. Rocci, L. Sorba, S. Roddaro, and V. S. Khrapai, Local noise in a diffusive conductor, *Sci. Rep.* **6**, 30621 (2016).
- [69] E. S. Tikhonov, Noise thermometry applied to thermoelectric measurements in InAs nanowires, *Semicond. Sci. Technol.* **31**, 104001 (2016).
- [70] M. J. M. de Jong and C. Beenakker, Semiclassical theory of shot noise in mesoscopic conductors, *Physica A* **230**, 219 (1996).

- [71] E. Pinsolle, A. Rousseau, C. Lupien, and B. Reulet, Direct measurement of the electron energy relaxation dynamics in metallic wires, *Phys. Rev. Lett.* **116**, 236601 (2016).
- [72] J. I. Väyrynen, D. I. Pikulin, and R. M. Lutchyn, Majorana signatures in charge transport through a topological superconducting double-island system, *Phys. Rev. B* **103**, 205427 (2021).
- [73] A. Ibabe, G. O. Steffensen, I. Casal, M. Gomez, T. Kanne, J. Nygard, A. L. Yeyati, and E. J. H. Lee, Heat dissipation mechanisms in hybrid superconductor-semiconductor devices revealed by Joule spectroscopy, [arXiv:2311.13229](https://arxiv.org/abs/2311.13229).
- [74] D. Ruhstorfer, A. Lang, S. Matich, M. Döblinger, H. Riedl, J. J. Finley, and G. Koblmüller, Growth dynamics and compositional structure in periodic InAsSb nanowire arrays on Si (111) grown by selective area molecular beam epitaxy, *Nanotechnology* **32**, 135604 (2021).
- [75] F. Del Giudice, J. Becker, C. De Rose, M. Döblinger, D. Ruhstorfer, L. Suomenniemi, J. Treu, H. Riedl, J. J. Finley, and G. Koblmüller, Ultrathin catalyst-free InAs nanowires on silicon with distinct 1D sub-band transport properties, *Nanoscale* **12**, 21857 (2020).
- [76] D. Rudolph, S. Funk, M. Döblinger, S. Morkötter, S. Hertenberger, L. Schweickert, J. Becker, S. Matich, M. Bichler, D. Spirkoska, I. Zardo, J. J. Finley, G. Abstreiter, and G. Koblmüller, Spontaneous alloy composition ordering in GaAs-AlGaAs core-shell nanowires, *Nano Lett.* **13**, 1522 (2013).
- [77] E. S. Tikhonov, M. Yu. Melnikov, D. V. Shovkun, L. Sorba, G. Biasiol, and V. S. Khrapai, Nonlinear transport and noise thermometry in quasiclassical ballistic point contacts, *Phys. Rev. B* **90**, 161405(R) (2014).